

A MULTIPLE TARGET TRACKING FILTER FOR NON-COOPERATIVE SPACE OBJECTS

G. Escribano⁽¹⁾, B. A. Jones⁽²⁾, M. Sanjurjo-Rivo⁽³⁾, J. A. Siminski⁽⁴⁾, A. Pastor⁽⁵⁾, and D. Escobar⁽⁵⁾

⁽¹⁾University Carlos III of Madrid, Av. de la Universidad 30, Leganés, Spain, Email: guescrib@ing.uc3m.es

⁽²⁾University of Texas at Austin, 2167 Wichita Street, Austin, Texas, Email: brandon.jones@utexas.edu

⁽³⁾University Carlos III of Madrid, Av. de la Universidad 30, Leganés, Spain, Email: msanjurj@ing.uc3m.es

⁽⁴⁾Space Debris Office, Robert-Bosch Strasse 5, Darmstadt, Germany, Email: Jan.Siminski@esa.int

⁽⁵⁾GMV, 11 Isaac Newton, Tres Cantos, Spain, Email: {apastor,descobar}@gmv.com

ABSTRACT

Space Surveillance and Tracking is central to the continuation of near Earth operations. Relying mainly on operator-specific and surveillance data, catalog maintenance integrity is highly sensitive to unknown maneuvers. Within this work we propose a method to limit the impact of non-cooperative targets on catalog maintenance and build-up activities based on state-of-the-art multi-target filtering and efficient control metrics.

Keywords: Multi target tracking, Maneuver detection, control distance metric, data association.

1. INTRODUCTION

The democratization of space access increases the demand for high quality Space Situational Awareness (SSA) services. Mission analysis and collision risk assessment necessitate accurate orbital population knowledge, typically stored in the form of space object catalogs [13]. To comply with some minimum requirements in orbital accuracy and timeliness, a vast surveillance network needs to be paired with capable sensor tasking and data processing algorithms. At the core of such algorithms is the observation-correlation process, through which the state of known (or newly detected) objects is updated based on incoming measurements of unknown origin.

The vastness of the orbital space and the high development and operating costs of sensor infrastructure result in relatively long re-observation times, adversely affecting the quality of tracking data. In addition, and due to Earth orbit being a highly demanded strategic asset, the data association problem is further complicated by non-cooperative maneuverable spacecraft. Automated means to identify and estimate unknown maneuvers is a strong requirement for capable Space Surveillance and Tracking (SST) cataloguing systems. In addition, an ideal SST algorithm should be able to properly identify new launches,

object re-entries, break-up events and spacecraft maneuvers.

A statistical framework that naturally allows for a time-varying population cardinality was presented by Mahler [8], under the concept of Finite Set Statistics (FISST). This framework deals with the definition of Random Finite Sets (RFS), which can be thought of as a random variable over all finite subsets of the state space, e.g., a set of random state vectors where the number of vectors is also random. The concept of RFS soon attracted the Multiple-Target Tracking (MTT) community, resulting in the development of novel multi-object filters, such as the Probability Hypothesis Density (PHD) [9] and Generalized Labeled Multi-Bernoulli (GLMB) [15]. The latter has seen a broad acceptance within the tracking community as it provides a full history of object tracks via a closed form solution (conjugate prior) in the presence of undetected objects, false observations, and object birth. Thereafter, under any possible data association scenario, the multi-object state will always be (backward) traceable and take the form of a GLMB distribution.

Implementations of the GLMB filter for maneuvering targets, or more generally, Jump Markov Systems (JMS), are already available in the literature [11, 12]. Common approximations for unknown maneuver dynamics consider the use of equivalent process noise [5], or adaptive model estimates based on optimal control [6]. While the former provides a computationally efficient approximation to unknown dynamics, its applicability to the space environment is limited due to the highly non-linear nature of orbital motion, e.g. changes to apoapsis altitude are more efficient near the periapsis. Approaches based on optimal control, on the contrary, present high computational demands that confront with the combinatorial nature of MTT. Within this work, we propose to bridge the gap between these two alternatives through the use of computationally efficient control distance metrics [3, 4]. Unknown maneuvers will then be characterized in terms of control metrics that rely on approximate dynamical models, which are still capable of capturing the main physics underlying orbital motion. A simulated space

surveillance scenario is used to evaluate the performance of the proposed multiple maneuvering target tracking filter implementation, with a particular focus on data association ambiguity and post-maneuver state estimation consistency.

2. GLMB FILTER FOR ACTIVE SPACECRAFT

The multi-target state of a given population of space objects, referred to a certain reference epoch, can be denoted as

$$\mathbf{X} = \{\mathbf{x}_1 \ \mathbf{x}_2 \ \dots \ \mathbf{x}_n\}, \quad \mathbf{x} = \{x \ m \ \ell\}, \quad (1)$$

with the single-target state $x \in \mathbb{R}^d$ being defined on the Cartesian position \bar{r} and velocity \bar{v} spaces, $m \in \mathbb{M}$ being the dynamical mode in effect and $\ell \in \mathbb{L}_{0:k} \equiv \mathbb{L}_{0:k-1} \cup \mathbb{L}_k$ a distinctive label used to differentiate each individual target. Within this work, we adopt Mahler's Finite Set Statistics [8] and model the multi-object state \mathbf{X} as a Random Finite Set, this is, a randomly sized collection of (random) state vectors \mathbf{x} . In what follows, the function $\mathcal{F}(\mathcal{S})$ is used to denote all the finite subsets of some space \mathcal{S} . Note that for the labels of a multi-target state \mathbf{X} to be unique, the cardinality $|\mathbf{X}| = n$ of the state and its set of labels, denoted as $\mathcal{L}(\mathbf{X})$, need to coincide. The unique label indicator is thus defined as

$$\Delta(\mathbf{X}) = \delta_{|\mathbf{X}|} [|\mathcal{L}(\mathbf{X})|], \quad (2)$$

where $\delta_x [y]$ is the Kronecker delta, thus returning a value of 1 if and only if $x = y$ and 0 otherwise. Let us also define the indicator function as

$$1_{\mathbb{X}}(x) = \begin{cases} 1 & \text{if } x \in \mathbb{X}, \\ 0 & \text{otherwise.} \end{cases} \quad (3)$$

Given a density function f defined over the single object state, it is common to express the multi-object exponential as

$$[f]^{\mathbf{X}} = \prod_{\mathbf{x} \in \mathbf{X}} f(\mathbf{x}), \quad (4)$$

with $[f]^{\emptyset} = 1$ by convention. In the following, we adopt the standard inner product notation

$$\langle f, g \rangle = \int f(x)g(x)dx, \quad (5)$$

where f and g are two real functions. Provided a set simultaneous observations $Z = \{z_1, z_2, \dots, z_{n_z}\}$, let $\theta : \mathbb{L} \rightarrow \{0, 1, \dots, |Z|\}$ indicate a one-to-one correspondence between target ℓ and an individual observation $\theta(\ell) \in \{1, \dots, |Z|\}$ or a missed detection $\theta(\ell) = 0$.

Vo et al. [15] propose to model the multi-target state at time t_k as a Generalized Labeled Multi Bernoulli (GLMB) distribution

$$\pi_k(\mathbf{X}) = \Delta(\mathbf{X}) \sum_{(I, \xi) \in \mathcal{F}(\mathbb{L}) \times \Xi} \omega_k^{(I, \xi)} \delta_I(\mathcal{L}(\mathbf{X})) \left[p_k^{(\xi)} \right]^{\mathbf{X}}, \quad (6)$$

where $\xi \in \Xi$ represents a hypothesis for the history of associations $\xi = \theta_{0:k}$, hypothesis weights $\omega_k^{(I, \xi)}$ are non-negative and satisfy

$$\sum_{(I, \xi) \in \mathcal{F}(\mathbb{L}) \times \Xi} \omega_k^{(I, \xi)} = 1, \quad (7)$$

and every $p_k^{(\xi)}$ is a valid Probability Density Function (PDF) defined over the single-target state space \mathbf{x} . The main advantage of this type of multi-object distribution is that it remains unchanged in the event of target birth, death, missed detections and clutter after the measurement update, yet still allowing for the recovery of individual target trajectories via the unique labels.

2.1. Filter Equations

Hereafter, we propose a definition of the GLMB filter tailored to the special characteristics of non-cooperative maneuvering targets in a space surveillance environment. Different GLMB filters for Jump Markov Systems can be found in the literature: Ravago et al. [12] propose to hypothesize over the event of a maneuver, performing maneuver detection via adaptive process noise and estimating the post-maneuver state by means of optimization methods; alternatively, PUNCHIHEWA [11] considers the dynamical mode to be part of the state space, thus resulting in a multi-modal single target density. Note that by considering maneuver detection to be part of the hypothesis generation process entails an additional layer of complexity when solving the assignment problem, this being the main reason why we adopt PUNCHIHEWA's formulation in the following. Accordingly, mode detection is implicit in the filtering process and can be recovered by evaluating the probability of a mode being active at certain time stamp, relieving the hypothesis generation from maneuver detection, thereby reduce the maximum number of hypothesis required to capture the true data association.

The joint prediction and update equation of the GLMB filter is provided in Eq. (8), where $I \in \mathcal{F}(\mathbb{L})$ represents the prior label set, $\xi \in \Xi$ is the history of data association hypotheses up to t_k , and $I_+ \in \mathcal{F}(\mathbb{L}_+)$ and $\theta_+ \in \Theta_+(I_+)$ indicate the filtered label set and association maps at the current filtering epoch t_{k+1} . The main filtering equation, Eq. (8) is complemented by expressions in Eqs. (9-17). Therein, the probability that target $\{x_+, \ell\}$ is alive at time t_{k+1} following dynamical mode m is denoted by $P_S^{(m)}(x_+, \ell)$. $r_{B,+}(\ell)$ represents the probability of a target being born. $P_D^{(m)}(x_+, \ell)$ is used to express the probability that a given sensor is able to detect target $\{x_+, \ell\}$ provided it is located within the sensor's Field of View (FOV), and is referred to as the probability of detection. Clutter measurements are modeled by the clutter intensity function $\kappa(z_j)$, effectively used to introduce false detections.

$$\pi(\mathbf{X}_+|Z_+) \propto \Delta(\mathbf{X}_+) \sum_{I,\xi,I_+,\theta_+} \omega^{(I,\xi)} \omega_{Z_+}^{(I,\xi,I_+,\theta_+)} \delta_{I_+} [\mathcal{L}(\mathbf{X}_+)] \left[p_{Z_+}^{(\xi,\theta_+)} \right]^{\mathbf{X}_+} \quad (8)$$

$$\omega_{Z_+}^{(I,\xi,I_+,\theta_+)} \propto \left[1 - \bar{P}_S^{(\xi)} \right]^{I \setminus I_+} \left[\bar{P}_S^{(\xi)} \right]^{I \cap I_+} \left[1 - r_{B,+} \right]^{\mathbb{B}_+ \setminus I_+} \left[r_{B,+} \right]^{\mathbb{B}_+ \cap I_+} \left[\bar{\psi}_{Z_+}^{(\xi,\theta_+)} \right] \quad (9)$$

$$\bar{P}_S^{(\xi)}(\ell) = \sum_{m \in \mathbb{M}} \bar{P}_S^{(\xi)}(m, \ell) \quad (10)$$

$$\bar{P}_S^{(\xi)}(m, \ell) = \left\langle p^{(\xi)}(\cdot, m, \ell), P_S^{(m)}(\cdot, \ell) \right\rangle \quad (11)$$

$$\bar{\psi}_{Z_+}^{(\xi,\theta_+)}(\ell) = \sum_{m_+ \in \mathbb{M}} \bar{\psi}_{Z_+}^{(\xi,\theta_+)}(m_+, \ell) \quad (12)$$

$$\bar{\psi}_{Z_+}^{(\xi,\theta_+)}(m_+, \ell) = \left\langle \bar{p}_+^{(\xi)}(\cdot, m_+, \ell), \psi_{Z_+}^{(\xi,\theta_+)}(\cdot, m_+, \ell) \right\rangle \quad (13)$$

$$\bar{p}_+^{(\xi)}(x_+, m_+, \ell) = \mathbf{1}_{\mathbb{B}_+}(\ell) p_B^{(m_+)}(x, \ell) + \quad (14)$$

$$\mathbf{1}_{\mathbb{L}}(\ell) \frac{\sum_{m \in \mathbb{M}} \vartheta(m_+|m) \left\langle P_S^{(m)}(\cdot, \ell) f_+^{(m_+)}(x_+|\cdot), p^{(\xi)}(\cdot, m, \ell) \right\rangle}{\bar{P}_S^{(\xi)}(\ell)} \quad (15)$$

$$p_{Z_+}^{(\xi,\theta_+)}(x_+, m_+, \ell) = \frac{\bar{p}_+^{(\xi)}(x_+, m_+, \ell) \psi_{Z_+}^{(\theta_+)}(x_+, m_+, \ell)}{\bar{\psi}_{Z_+}^{(\xi,\theta_+)}(m_+, \ell)} \quad (16)$$

$$\psi_{Z_{\{1:|Z|\}}}^{(j)}(x_+, m_+, \ell) = \begin{cases} \frac{P_D^{(m_+)}(x_+, \ell) g^{(m_+)}(z_j|x_+, \ell)}{\kappa(z_j) + \delta_0 [\kappa(z_j)]} & \text{if } j \in 1, \dots, |Z| \\ 1 - P_D^{(m_+)}(x_+, \ell) & \text{if } j = 0 \end{cases} \quad (17)$$

The likelihood that observation z corresponds to state x under dynamical mode m is represented by $g^{(m)}(z|x, \ell)$, and corresponds to the usual measurement likelihood. $\vartheta(m_+|m)$ indicates the probability that mode m_+ is active in the time interval $[t_k, t_{k+1}]$ conditioned on the fact that mode m was active during $[t_{k-1}, t_k]$.

The transition density $f_+^{(m_+)}(x_+|x)$, which satisfies the Chapman-Kolmogorov equation, is defined for the ballistic $m = 0$ and maneuver $m = 1$ modes as

$$f_+^{(m_+)}(x_+|x) = \begin{cases} f^{(0)}(x_+|x) & \text{if } m_+ = 0, \\ \frac{\phi(x_+, x)}{\bar{\phi}(x)} & \text{if } m_+ = 1, \end{cases} \quad (18)$$

where $f^{(0)}(x_+|x)$ corresponds to a natural dynamical model in the near Earth environment and

$$\phi(x_+, x) = \begin{cases} 1 & \text{if } P(x_+, x) \leq P_{adm}, \\ 0 & \text{if } P(x_+, x) > P_{adm}, \end{cases} \quad (19)$$

$$\bar{\phi}(x) = \int \phi(x_+, x) dx_+, \quad (20)$$

i.e. the maneuver transition density is modeled as a uniform distribution over the reachable set. This set is defined in terms of some control measure $P(x_+, x)$, following the approach proposed by Holzinger et al. [6],

and serves the purpose of evaluating the control effort required to transfer between a prior x and a posterior x_+ orbital state. To ensure the transition is a proper density, it is required to include some normalization constant $\bar{\phi}(x)$ that corresponds to the hypervolume of the reachable set, the latter being defined by the set of states whose control distance metric to some prior orbit falls below some admissible threshold P_{adm} . Note the proposed dynamics for the maneuver mode simply depends on a single parameter with a strong physical meaning: the maximum maneuvering capability of the target. Thus, the filter allows to consistently represent the state PDF in the absence of additional maneuver data, sequentially adapting the uncertainty as more observations are received.

3. FILTER IMPLEMENTATION

As discussed in [14] the GLMB is an exact filter, yet a complete implementation is often intractable as the number of data association hypotheses to be considered grows unbounded. To mitigate this, it is common practice to truncate hypotheses based on their relative weights and also to set an upper bound n_H on the number of parallel hypotheses to be considered. Note the latter plays a crucial role on the accuracy of the filter since such number needs to be sufficiently large to keep the true association hypothesis alive at all times. In this regard, one can make use of Murty's algorithm [10] to solve the ranked assignment problem, i.e. determine a sorted list of measurement

to object association hypotheses. For complex cases with high dimensionality, alternative methods based on Gibbs sampling can be used to find an approximate solution to the ranked assignment problem, though the devised test case consider a moderate number of targets and thus the current implementation uses Murty’s algorithm.

Tractability not only concerns multi-object but also single target state space filtering, in particular for any system undergoing non-linear transformations. There exists multiple approaches to perform filtering on non-linear systems, which are based on different assumptions. The most general techniques, such as Particle Filtering (PF) and Markov Chain Monte Carlo (MCMC), express probability densities in sampled form, thus being able to approximate any type of distribution provided the number of samples is large enough. Note, however, that for high dimensional systems the number of samples required to ensure certain level of similarity with the true distribution grows exponentially with the state dimension, so this type of methods rapidly become intractable. To overcome these limitations, there are a number of methods that assume the posterior to pertain to certain family of distributions, typically Gaussian, and usually match the first and second order moments: some examples are the Extended Kalman Filter (EKF) and the Unscented Kalman Filter (UKF). Still, the accuracy of this techniques highly depends on the divergence of the true density from the assumed form. There exists some methods aimed at combining the computational efficiency of assumed distributions and the flexibility of sampling-based approaches, most of which rely on mixture distributions. In the Gaussian Sum Filter (GSF) [7], for instance, the PDF is modeled as a sum of Gaussians, also known as Gaussian Mixture Model (GMM), each with a support sufficiently small so that the filtering process can be approximated as linear. Thus, one can perform a Kalman update on each GMM component to obtain a tractable approximation for the posterior density. One of the key aspects of these type of approaches is the need to detect whenever a component deviates from its assumed shape under certain non-linear transformation, and split it accordingly to minimize the divergence. The Adaptive Entropy-based Information Synthesis (AEGIS) method [1] provides a solution to this particular problem by monitoring the differential entropy during uncertainty propagation and splitting individual components whenever the linearization error, as indicated by an increase in entropy, transcends a given threshold.

For space objects tracking applications, both the measurement and dynamical models typically shown strong non-linearities, especially considering the long revisit times that characterize surveillance scenarios. In addition, the definition of the maneuver dynamics given in the previous section imply a support of a considerable size, whose uncertainty propagation would require some type of splitting. Thus, we propose to use a GSF with AEGIS uncertainty propagation to combine the benefit of sampled densities for non-linear mappings and the closed form inference enabled by linear Gaussian assumptions in the reduced support components.

3.1. Maneuver dynamics

In the absence of prior information regarding certain maneuver, a common hypothesis is to assume fuel or energy optimality. This is a reasonable approach when the post-maneuver state of the system is well-defined, but can lead to significant biases for partially observed systems. To overcome this limitation, the maneuver transition density can be modeled as a uniform prior (see Eqs.(18-20)) over some reachable set, i.e. the space accessible to the target conditioned on an expected control performance. In line with the filtering scheme proposed in the previous section, it is possible to approximate such uniform distribution by a GMM [2], whose individual components can then be propagated via AEGIS and updated using some Kalman-type approach. Recalling the accuracy of a linear (Kalman) update is affected by the validity of the linear assumption within the support of the Gaussian, both in the state and measurement spaces, the covariance of each individual component shall be sufficiently small. These requirements are mostly related to the non-linear measurement model, since the AEGIS propagator is capable of automatically splitting those components whose distribution deviates from Gaussian. In any case, these requirements can hinder the tractability of the method since the required number of components can be in the order of tens of thousands for every individual target.

Instantiating only those components that are in the support of a hypothesized observation can significantly reduce the computational and storage requirements, while still allowing to characterizing the posterior distribution. Accordingly, we propose the following procedure to approximate the single object density in the event of a maneuver:

1. The density of a target is expressed as

$$p(x) \approx \sum_{i=1}^{n_C} w_i \mathcal{N}(x; \mu_i, \Sigma_i), \quad (21)$$

being w_i the weight associated to Gaussian component with mean μ_i and covariance Σ_i . An assumption regarding the control distance metric is that the covariance shall be sufficiently small so that the distance between some point and a Gaussian component can be approximated by the deterministic distance to the component mean. Note otherwise the control measure would follow some a priori unknown distribution, adding an additional layer of complexity.

2. The reachable set

$$\mathcal{R}(x_+; x) = \{x_+ : P(x_+, x) \leq P_{adm}\} \quad (22)$$

is approximated by the polytope

$$\mathcal{R}(x_+; x) \approx \mathcal{R}'(x_+; \hat{x}, b_r, n_r), \quad (23)$$

where the scalars b_r and directions n_r satisfy

$$P(\hat{x} + b_r n_r, x) = P_{adm}. \quad (24)$$

Recall that the state density is expressed as a Gaussian mixture, and hence the reachable set takes the form of a weighted mixture

$$\mathcal{R}(x_+; x) = \bigcup_{i=1}^{n_C} \mathcal{R}(x_+; \mu_i) \quad (25)$$

with a weight w_i assigned to each individual set $\mathcal{R}(x_+; \mu_i)$.

3. As discussed earlier, the reachable set is only used to determine the maneuver transition density, since the post-maneuver state distribution is directly conditioned on certain measurement. This reduced set, termed the admissible control region, is formally expressed as

$$\mathcal{C}(x_+; x, z) = \mathcal{R}(x_+; x) \cap \text{supp}(g(z|x_+)), \quad (26)$$

and can be approximated by some polytope

$$\mathcal{C}(x_+; x, z) \approx \mathcal{C}'(x_+; x, z, x_+^*, b_c, n_c). \quad (27)$$

Therein, the centroid of the admissible region x_+^* is defined by

$$x_+^* = \left\{ x_+ : \underset{x_+}{\text{argmin}} [P(x_+, x)], g(z|x_+) \geq p_\alpha \right\}, \quad (28)$$

which is used to find a set of search directions n_c and magnitudes b_c that satisfy the condition

$$P(x_+^* + b_c n_c, x) = P_{adm} \quad (29)$$

or

$$g(z|x_+^* + b_c n_c) = p_\alpha, \quad (30)$$

whichever results in a lower b_c .

4. DeMars et al. [2] proposed a method to approximate a uniform distribution with a GMM, providing optimal covariance values as a function of the grid size. Each individual component is assigned a weight that is proportional to the volume it represents with regard to the uniform distribution. Due to the adoption of a multi-modal distribution for $p(x)$, and analogous to the reachable set, the admissible control region in the previous step is also given by a mixture. The weight associated to each individual Gaussian component that approximate this set is computed as

$$w_j^+ = \frac{\sum_{i=1}^{n_C} \int \mathcal{R}'(x_+, \mu_i) dx_+ \sqrt{2\pi^d \det(\Sigma_j^+)}}{\int \mathcal{R}'(x_+, \mu_i) dx_+} w_i \phi(\mu_j^+, \mu_i), \quad (31)$$

and the prior post-maneuver state distribution reads

$$p(x_+) = \sum_{j=1}^{n_{C+}} w_j^+ \mathcal{N}(x_+; \mu_j^+, \Sigma_j^+). \quad (32)$$

Therefore, each component is assigned a weight that is proportional to the volumetric ratio between its representative space $\sqrt{2\pi^d \det(\Sigma_j^+)}$ and the individual reachable set $\int \mathcal{R}'(x_+, \mu_i) dx_+$, multiplied by the weight associated to said prior component w_i .

4. NUMERICAL STUDY

4.1. Test case definition

Multiple target tracking filters are specifically tailored to operate with high ambiguity levels, for instance in cluttered regions with closely spaced targets. One of such scenarios is typical in the Geostationary ring, where operational satellites are assigned a tight longitude slot. Station keeping maneuvers are thus frequently performed in order to comply with such requirement, and oftentimes satellites can appear close in the observation space. To mimic this environment, we have developed a test case involving 10 Geostationary spacecraft, wherein 3 objects perform impulsive maneuvers to approach another three targets. These two burns, featuring a $\Delta V_{1,2} \sim \mathcal{U}(0.5, 1.0)$ m/s along a random direction, are executed during two separate time windows $t_{m,1} \in [11, 14]$ and $t_{m,2} \in [17, 20]$ elapsed hours, which correspond to the first (daytime) blackout interval for an optical survey. After the two-impulse maneuver, the *chaser* satellites are placed at a distance $\Delta r \sim \mathcal{U}(200, 1000)$ m from their corresponding *targets*. Figure 1 shows the evolution of the semi-major axis as a function of the mean longitude for one of the Monte Carlo trials, wherein one can appreciate the small relative distance between the *chasers* and *targets*. Measurements are modeled as optical attributes obtained from a single telescope every 4 hours (during nighttime only), with an angular accuracy $\sigma_{\alpha,\delta} = 1$ arcsec and $\sigma_{\dot{\alpha},\dot{\delta}} = 0.1$ arcsec/s. The total propagation time is 5 days to allow for the post-maneuver state estimates to converge to reasonable uncertainty levels for, e.g. collision screening purposes. Figure 2 depicts the observation and maneuver sequence for a representative Monte Carlo trial, where it is shown that the filter receives three observations per night for each object. The natural dynamical model employed for the simulation considers the Sun and Moon as third bodies, a cannonball model for the solar radiation pressure and a non-spherical Earth model of degree and order 8.

Implemented in C++, the tested filter presents the following configuration:

- Probability of detection $P_D^{(m)}(x, \ell) = 1 - 10^{-3}$.
- Probability of survival $P_S^{(m)}(x, \ell) = 1 - 10^{-7}$.
- Probability of maneuver $\vartheta(m_+|m) = 0.01$.
- No birth, clutter or missed detections are considered to focus on the impact of the maneuvers themselves.
- Minimum relative hypothesis weight $\omega_{min} = 10^{-7}$.
- Maximum number of considered hypotheses $n_H = 50$.
- Measurement gate for data association $d_G = 6.0$ in the Mahalanobis distance.

- Individual component covariances are inflated with a process noise $\sigma_a = 10^{-8} \text{ m/s}^2$ during propagation, thus affecting AEGIS splitting.
- We used the efficient (impulsive) control metric derived in 3, with a maximum expected control $P_{adm} = 5 \text{ m/s}$.
- Single target inference is performed using an Unscented Kalman Filter scheme for each component mixture.

4.2. Results and discussion

Evaluation of the filter is mainly focused on the data association performance of the proposed GLMB filter, though single target consistency is also evaluated. The code failed at retrieving test case IV results, presumably due to corrupted data or incompatibilities between the GM single-target density and the HDF5 format used to extract the filter output, but there are still 9 Monte Carlo trials from which to infer some statistics. Each individual test case run for 8.2 hours on average, parallelizing the individual measurement to object computations using separate CPU threads. Note the main share of the workload corresponds to control metric evaluations, i.e. finding the reachable sets and the admissible control regions, accounting for about $\sim 95\%$ since these need to be computed for each individual GM component. Thus, efficient parallelization in this regard, e.g. using GPGPU programming, is expected to significantly reduce the algorithm runtimes.

Data association errors, considered as any type of incorrect individual observation to object mapping, are gathered in Table 1 for the sequential output and top 5 surviving hypotheses. Cross tagging is the main data association error type, though there are some missed detections as indicated by odd error counts. Figure 3 presents the evolution of the instantaneous sequential data association error counts for the different test cases considered. Therein, one can see that the majority of these errors are due to a cross correlation between two targets, in fact,

the mistaken targets are two *chasers* whose trajectories intersect. Note the developed algorithm is unable to distinguish these two targets since their reachable sets intersect, and since the maneuver transition density is uniform, the two possible data association maps are equally likely. Note one could artificially resolve this issue by favouring *optimal* transfers, this is, giving higher credit to lower control metric transfers. However, this potentially results in a biased filter since the goal of each target's maneuver is a priori unknown. Another source of data association errors is found at the first post-maneuver observation frame, where *chasers* and *targets* are likely to be cross tagged due to their proximity. In any case, it can be argued that the proposed filter is not able to recover the true data association sequence for any of the test cases considered, at least in the top 5 hypotheses. While this holds true, one should recall the complexity of the

proposed test case, with several intersecting target trajectories and unknown double burn maneuvers on the order of 1-2 m/s .

In fact, and as indicated by Figure 4, the algorithm maintains custody of the complete target population. This figure shows the evolution of the Optimal Sub-Pattern Assignment metric, defined for a set of estimated \mathbf{X} and reference \mathbf{X}^* targets and as in Eq. (4.2), being Γ_n the set of all permutations $\{1, \dots, n\}$, for $n \in \mathbb{N}$ and $\gamma \in \Gamma_n$ a sequence $\{\gamma(1), \dots, \gamma(n)\}$. The distance $d_c(\mathbf{x}_i, \mathbf{x}_{\gamma(i)}^*) = \min(c, d(\mathbf{x}_i, \mathbf{x}_{\gamma(i)}^*))$ represents the minimum between a cut-off c and a base distance $d(\cdot, \cdot)$. A common decision in multi-target tracking is to use the Cartesian position distance as $d(\cdot, \cdot)$, and so is done in this work, together with a cutoff parameter $c = 100 \text{ km}$ and order $p = 2$. Note the single target density is given by a GMM, and so the distance is computed as a weighted sum across all the different components. Seven cases present a maximum OSPA below 20 km , and from the two remaining cases one converges in a reasonable amount of time. Convergence in the worst case is delayed until the fourth day, and we attribute this to the reduced observability implied by the use of a single surveillance sensor, typically presenting ambiguity in between the inclination and semi-major axis / eccentricity.

$$D(\mathbf{X}, \mathbf{X}^*) = \left[\frac{1}{|\mathbf{X}|} \left(\min_{\gamma \in \Gamma_{|\mathbf{X}^*|}} \sum_{i=1}^{|\mathbf{X}|} d_c(\mathbf{x}_i, \mathbf{x}_{\gamma(i)}^*) + (|\mathbf{X}^*| - |\mathbf{X}|) \cdot c^p \right) \right]^{\frac{1}{p}} \quad (33)$$

Besides the state estimation error in absolute terms, somehow provided by the OSPA metric, it is of interest to evaluate the single target filtering consistency. In doing this, we propose to use the Scaled Normalized Estimation Error Squared (SNEES)

$$SNEES = \sum_{i=1}^{n_C} \frac{w_i}{d} (E[x_i] - x_i^*)^T Cov[x_i]^{-1} (E[x_i] - x_i^*),$$

applied to a Gaussian mixture via a weighted sum. The OSPA metric indicated a relatively high state estimation

error, on the order of tens of kilometers, but the consistency metric shows there is no evidence to lower such error without biasing the filter, at least with no prior knowledge on the maneuver characteristics. For the most part, the SNEES of the maneuvering targets remains in the vicinity of 1, which happens to be the optimal value, as depicted in Figure 5. There are, however, three distinguishable peaks with a value exceeding 20, which correspond to state estimates in the tail of the uniform maneuver prior. This indicates certain level of inconsistency in the filtered estimate, but the filter is still able to overcome

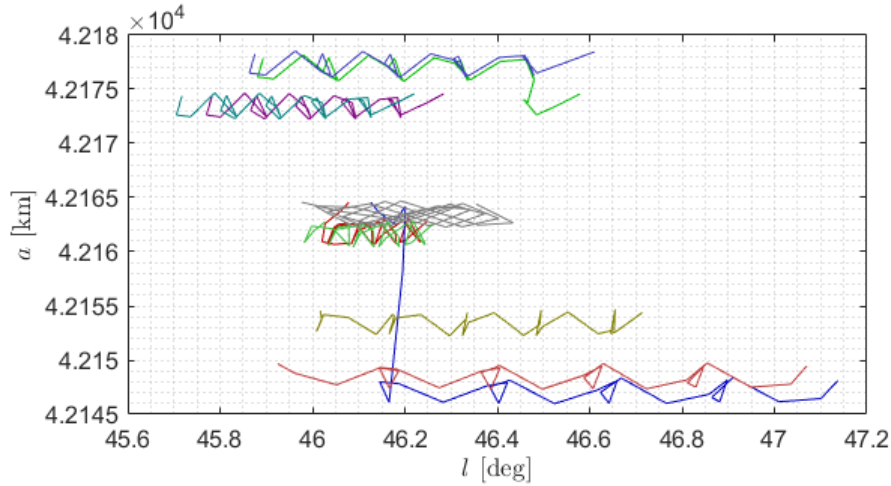


Figure 1. Semi-major axis vs mean longitude evolution for one of the Monte Carlo trials.

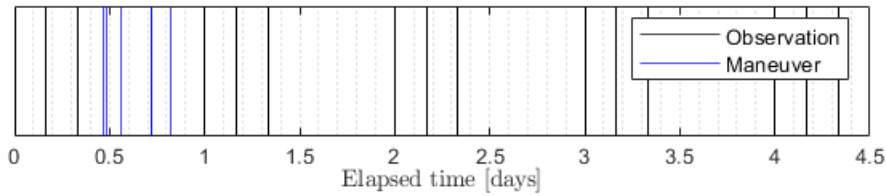


Figure 2. Measurement and maneuver sequence for one of the Monte Carlo trials.

this by sequentially pruning the mixture components that are far from the true state, finally converging to a consistent estimate. This suggests that care must be taken when extracting the state in early post-maneuver epochs, since the support of the density may present a complex behavior. Still, since custody is maintained, an operator could task a tracking-type sensor to resolve the ambiguity caused by the detected maneuver, thus potentially resolving any data association conflict.

5. CONCLUSIONS

We have proposed a Generalized Labeled Multi-Bernoulli filter to track uncooperative space objects. The single target space is augmented with the dynamical mode in effect during some propagation interval, with a binary mode space given by the natural uncontrolled dynamics and a uniform transition density in the space assumed accessible to the target. The latter is bounded by some maximum expected control effort, whose control magnitude should be in excess of the executed maneuvers in order to enhance the filter convergence and consistency. As a result, data association is not conditioned on the event of a maneuver, effectively reducing the number of hypothesis generated by the algorithm.

Our tractable implementation of the proposed scheme relies on efficient control metrics, which make use of approximate dynamical models to reduce the computational

complexity. Single target densities are modeled in a mixture form, as dictated by the mode-augmented state space. We have noted that this results in an added complexity as every individual component should be considered for reachability computations, yet the filter is kept tractable for a moderate number of targets and individual components on the order of hundreds.

Though not able to infer the true data association sequence for the selected test case, the algorithm has proved to maintain custody of the target population, showing adequate levels of consistency in the state estimates. Future work will explore the capabilities of the algorithm in more demanding scenarios, such as continuous low-thrust maneuvers in low Earth orbits, as well as improved methods for approximating both the reachable set and admissible control region.

ACKNOWLEDGMENTS

The work developed in this paper was funded by the European Space Agency as part of an ongoing PhD thesis through the Project *Combined Heuristic and Statistical Methodologies applied to Maneuver Detection in the SST Observation Correlation Process*, grant number 4000129944/20/D/MB, and also through grant TED2021-132099B-C33 funded by MCIN/AEI/10.13039/501100011033 and by “European Union NextGenerationEU/PRTR”. . The contribution of B.

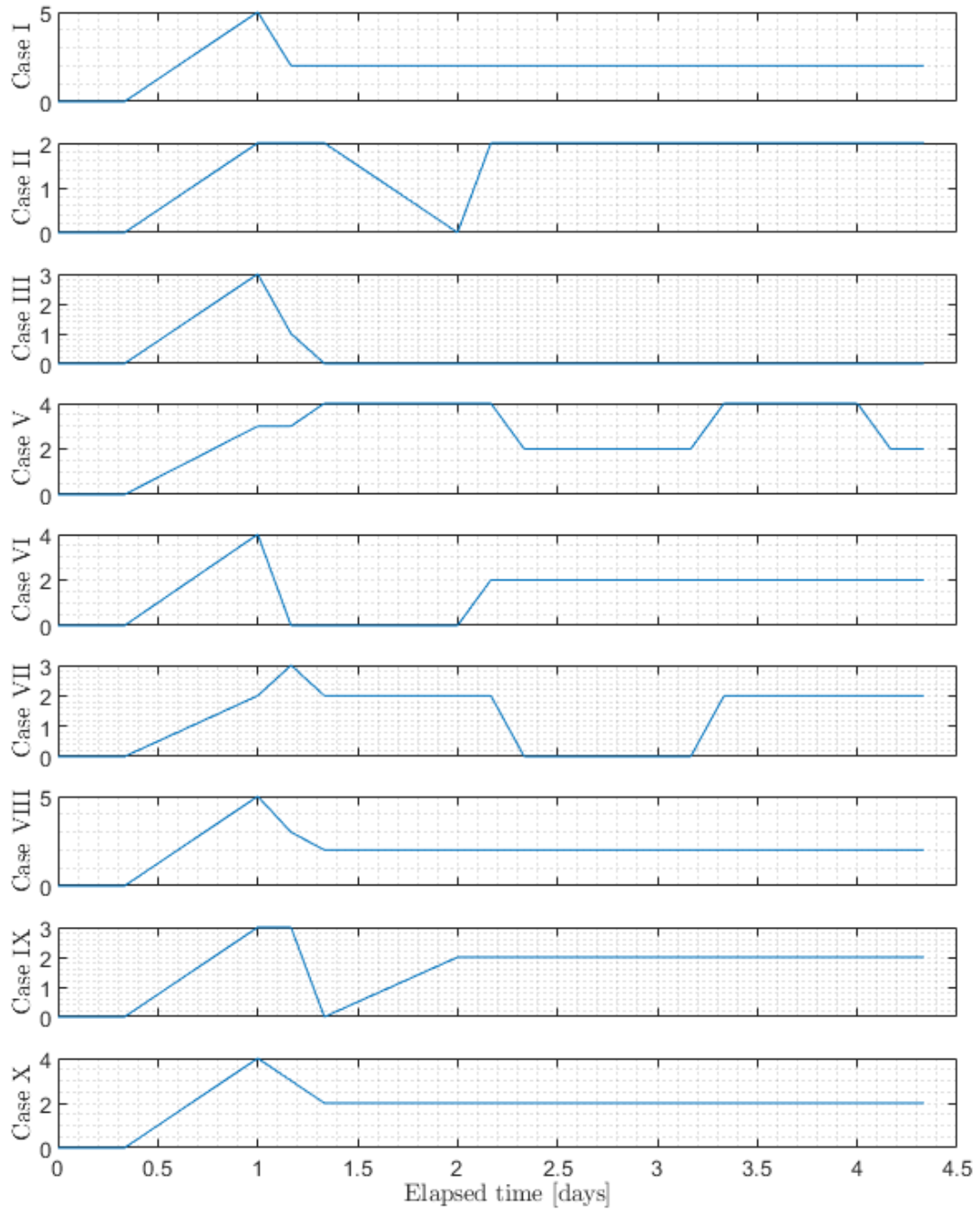


Figure 3. Data association error sequence for the different Monte Carlo trials.

Test Case	I	II	III	V	VI	VII	VIII	IX	X
Sequential	27	22	4	36	20	19	28	24	27
Hypothesis I	25	25	2	30	29	24	26	25	26
Hypothesis II	26	26	-	32	28	4	27	26	24
Hypothesis III	27	24	-	28	28	-	-	26	27
Hypothesis IV	4	-	-	48	27	-	-	27	27
Hypothesis V	-	-	-	27	30	-	-	28	-

Table 1. Data association errors for a total of 150 observations.

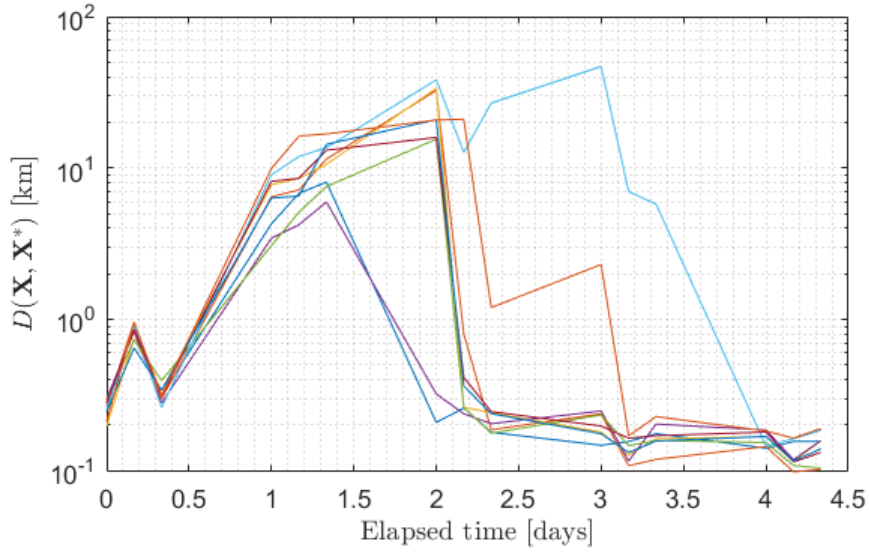


Figure 4. OSPA metric for the test cases considered.

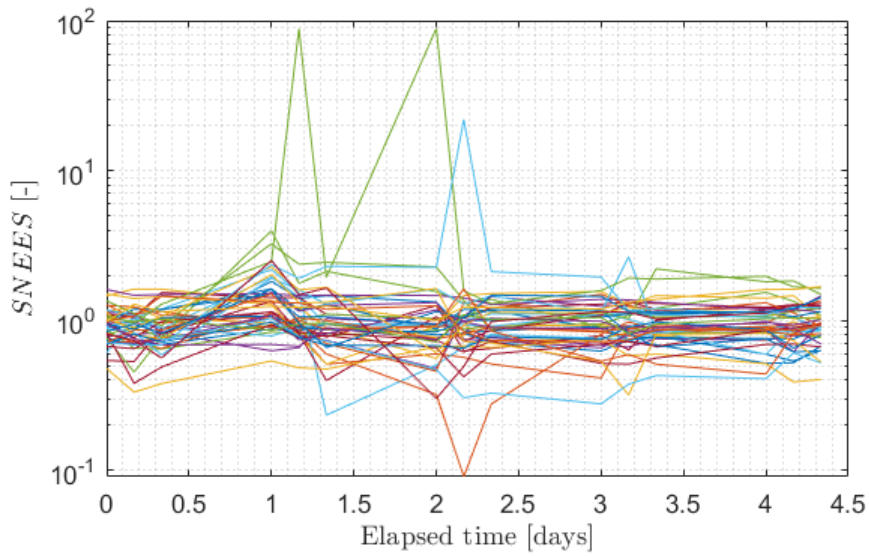


Figure 5. SNEES evolution for the three maneuvering targets.

Jones is supported by the Air Force Office of Scientific Research under award number FA9550-19-1-0404.

REFERENCES

1. Kyle J. DeMars, Robert H. Bishop, and Moriba K. Jah. Entropy-based approach for uncertainty propagation of nonlinear dynamical systems. *Journal of Guidance, Control, and Dynamics*, 36(4):1047–1057, 2013.
2. Kyle J. DeMars and Moriba K. Jah. Probabilistic initial orbit determination using gaussian mixture models. *Journal of Guidance, Control, and Dynamics*, 36(5):1324–1335, 2013.
3. G. Escribano, M. Sanjurjo-Rivo, J.A. Siminski, A. Pastor, and D. Escobar. Automatic maneuver detection and tracking of space objects in optical survey scenarios based on stochastic hybrid systems formulation. *Advances in Space Research*, 2022.
4. Guillermo Escribano, Alejandro Pastor, Jan Siminski, Diego Escobar, and Manuel Sanjurjo-Rivo. Data association for maneuvering space objects considering different control distance metrics. In *AIAA/AAS Astrodynamics Specialist Conference*, 2022.
5. Gary M. Goff, Johnathan T. Black, and Joseph A. Beck. Orbit estimation of a continuously thrusting spacecraft using variable dimension filters. *Journal of Guidance, Control, and Dynamics*, 38(12):2407–2420, 2015.
6. Marcus J. Holzinger, Daniel J. Scheeres, and Kyle T. Alfriend. Object correlation, maneuver detection, and characterization using control distance metrics. *Journal of Guidance, Control, and Dynamics*, 35(4):1312–1325, 2012.
7. Joshua T Horwood, Nathan D Aragon, and Aubrey B Poore. Gaussian sum filters for space surveillance: theory and simulations. *Journal of Guidance, Control, and Dynamics*, 34(6):1839–1851, 2011.
8. Ronald P. S. Mahler. Random-set approach to data fusion. In Firooz A. Sadjadi, editor, *Automatic Object Recognition IV*, volume 2234, pages 287 – 295. International Society for Optics and Photonics, SPIE, 1994.
9. R.P.S. Mahler. Multitarget bayes filtering via first-order multitarget moments. *IEEE Transactions on Aerospace and Electronic Systems*, 39(4):1152–1178, 2003.
10. Katta G. Murty. Letter to the editor—an algorithm for ranking all the assignments in order of increasing cost. *Operations Research*, 16(3):682–687, 1968.
11. Yuthika Punchihewa. Efficient generalized labeled multi-bernoulli filter for jump markov system. In *2017 International Conference on Control, Automation and Information Sciences (ICCAIS)*, pages 221–226, 2017.
12. Nicholas Ravago and Brandon A Jones. Tracking multiple maneuvering satellites using a generalized labeled multi-bernoulli filter. In *AIAA/AAS Astrodynamics Specialist Conference*, 2019.
13. Quentin Verspieren. The united states department of defense space situational awareness sharing program: Origins, development and drive towards transparency. *Journal of Space Safety Engineering*, 8(1):86–92, 2021.
14. Ba-Ngu Vo, Ba-Tuong Vo, and Hung Gia Hoang. An efficient implementation of the generalized labeled multi-bernoulli filter. *IEEE Transactions on Signal Processing*, 65(8):1975–1987, 2017.
15. Ba-Tuong Vo and Ba-Ngu Vo. Labeled random finite sets and multi-object conjugate priors. *IEEE Transactions on Signal Processing*, 61(13):3460–3475, 2013.